BAJOPMAS JOURNAL 16(1): 101 – 112
Printed in Bayero University, Kano - Nigeria.

DELINEATION OF RADIOACTIVE MINERALIZATION ZONES USING AIRBORNE MAGNETIC AND RADIOMETRIC DATA IN GANJUWA AREA OF BAUCHI STATE, NORTHEASTERN NIGERIA,

[1]Alkali, M. J.; [2]Ahmed, A. B.; [1*]Mansur, S.; [3]Muhammed, S.; [1]Abdullahi, M. G. and [1]Isa, M. B.
[1]Physics Department Northwest University Kano Nigeria
[2]Physics Department Gombe State University Nigeria
[3]Physics Department Bayero University Kano Nigeria
Email:mansursaid79@gmail.com

ABSTRACT
This study investigates radioactive mineralization through a detailed analysis of aeromagnetic and aero-radiometric data in Ganjuwa area, Bauchi State, Northeastern Nigeria. According to sheet-129, the study area is between latitudes 10°30'N and 11°00'N and longitudes 10°00'E and 10°30'E. Magnetic data analysis, including regional-residual separation and reduction to the equator, revealed a diverse magnetic landscape with intensities ranging from -201.97nT to 360.07nT. Structural enhancement techniques, such as analytic signal, First Vertical Derivative (FVD), Horizontal Gradient Magnitude (HGM), and Tilt Derivative (TDR), identified northeast-southwest (NE-SW) trending linear features. Euler deconvolution provided depth estimates between 122.47m and 1102.75m. High levels of potassium (K), equivalent thorium (eTh), and equivalent uranium (eU) were found in airborne radiometric data; these values ranged from 0.04% to 6.67% for K, 7.6 ppm to 124 ppm for eTh, and 2.07 ppm to 14.38 ppm for eU. These levels, though above global averages, remain within safe limits, suggesting localized zones of mineralization. The K/eTh ratio map highlighted significant hydrothermal activity in the southern and southwestern regions. Areas of potassium mineralization are located between latitudes 10°30'N to 10°47'N and longitudes 10°03'E to 10°22'E, with depths from 250m to 800m. Thorium and uranium mineralization zones are located between latitudes 10°30'N to 10°43'N and longitudes 10°00'E to 10°18'E, with depths from 130m to 750m. Hydrothermal alteration zones are between latitudes 10°32'N to 11°00'N and longitudes 10°04'E to 10°24'E, with depths from 250m to 800m. These findings highlight potential targets for further exploration and resource development, particularly for potassium, uranium, thorium, and valuable ores like gold, silver, and copper.

Keywords: Aeromagnetic Data, Composite, Dip, Euler, Inclination, Lineament, Radiometric Data, Source Parameter Imaging, Ternary

1.1 Introduction
Radioactive minerals encompass various elements that emit radiation due to their unstable atomic nuclei. Some of the most common radioactive minerals include uranium, thorium, and potassium-rich minerals like potassium-40 [1]. Igneous, sedimentary, and metamorphic rocks are among the geological formations that naturally contain radioactive materials in the Earth's crust [2]. Uranium is commonly found in sedimentary rocks like shale, sandstone, and limestone, as well as in igneous rocks like granite and pegmatite. Thorium is often found in monazite and other rare earth minerals, which can be found in igneous and metamorphic rocks. Potassium-40 is a common isotope found in various minerals, including feldspar and mica, which are present in igneous, sedimentary, and metamorphic rocks [3]. Radiometric method stands out as the primary geophysical technique employed for the direct exploration

of radioactive minerals [4]. However, as a means for enhancing the effectiveness of exploring these minerals, the radiometric method is often combined with other geophysical techniques like the magnetic method, gravity method, electromagnetic method and induced polarization.

In mineral exploration and regional tectonic research, airborne magnetic and radiometric geophysical surveys have been essential in determining the relevant physical characteristics of subsurface rock units over vast, typically inaccessible areas. The magnetic method helps in delineating geological structures, such as faults, folds, and intrusions, which play a crucial role in the concentration and localization of mineral deposits [5]. Many minerals of importance exhibit magnetic properties, and their occurrences are often structurally controlled. The variations in magnetic properties help in mapping lithological units and delineating subsurface structures that might host mineralization. Radiometric method, on the other hand, helps in identifying specific radioactive elements associated with potential mineral deposits. Different minerals exhibit distinctive radiometric signatures, and their concentration can indicate areas with economic mineralization [6]. This method assists in detecting hydrothermal alteration zones, which are often associated with geothermal potential and the formation of various mineral deposits, such as, gold copper and silver [7].

The geothermal potential of Northeastern Nigeria, particularly Bauchi State, has been extensively studied using magnetic, radiometric and remote sensing techniques as seen in [8], [9] and [10]. This potential is primarily attributed to the spontaneous decay of radioelements (Uranium, Thorium and Potassium), and their decay products like Radon and Radium [11]. These substances hold significant economic importance if explored, exploited, and effectively harnessed. However, there is a lack of widely reported investigations on the distribution and concentration of radioelements in the region.

In light of the foregoing, this study aims to investigate the distribution and concentration of Potassium (K), Uranium (U) and Thorium (Th) in Ganjuwa, Bauchi State, Northeastern Nigeria, for potential exploitation, using high resolution airborne magnetic and radiometric data of the area.

1.2 Location and Geology of the Study Area

The study area (Figure 1) which corresponds to sheet-129, is about 71km northeast of Bauchi capital of Bauchi state. The area lies between Latitudes 10°30`N to 11°00`N and Longitudes 10°00`E to 10°30`E. Ganjuwa has a tropical savannah climate, being warm every month with both wet and dry seasons. The average annual temperature for Ganjuwa is 35°C and has about 222 mm of rain in a year [12].

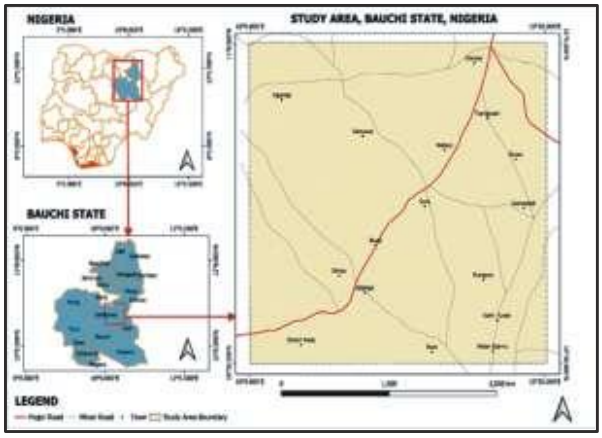

Figure 1: Location Map of the Study Area (Extracted and Modified on QGIS)

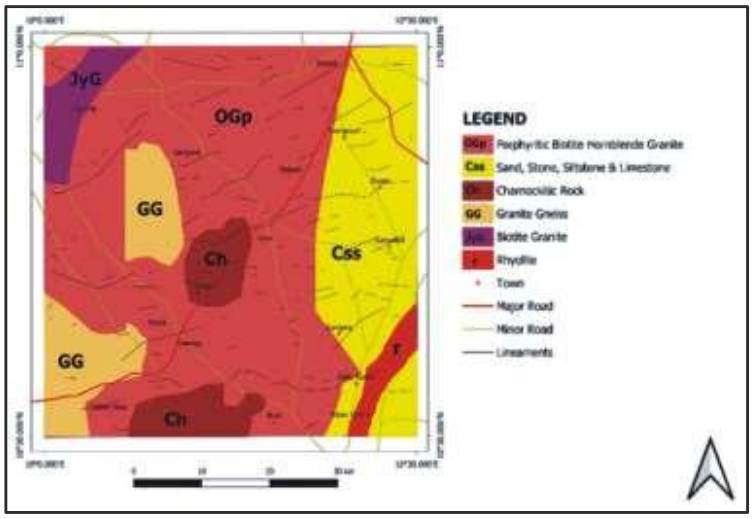

Figure 2: Geological Map of the Study Area (Extracted and Modified on QGIS)

The geological map of Ganjuwa, as shown in Figure 2, highlights a diverse range of rock types, each contributing to the area's geological complexity. Dominating about 70% of the study area is the Porphyritic biotite hornblende granite, which is part of the Pan-African older granitoids from the Precambrian to Cambrian period [13]. This type of granite signifies ancient geological formations that continue to influence the region's landscape. Additionally, Charnockitic rock, also from the Pan-African older granitoids, is present in the central and southern parts of the area, reinforcing the ancient geological context. Granite gneiss, a crucial element of the Migmatite-gneiss complex that dates from the Precambrian to Cambrian epoch, is what defines the eastern portion of the research area [13]. The map also reveals the presence of Cretaceous-Senonian sandstone, siltstone, and limestone from the Chad formation, which overlay the older crystalline basement rocks [13]. These sedimentary rocks provide insights into ancient depositional environments. Furthermore, the NW and SE corners of the study area feature biotite granite and rhyolite, respectively, classified as Pan-African younger granitoids with a Jurassic age [13]. These younger granitoids represent a subsequent phase of magmatic activity, reflecting the region's evolving geological history.

2.1 Theoretical Background

2.1.1 Magnetic and Radiometric Methods

Any magnetic grain is a dipole. That is, it has two monopoles, m_1 and m_2 of opposite signs directly linked together. Magnetic prospecting is based on the presence of these magnetic dipoles or monopoles within Earth's rocks [14]. For a force between two magnetic monopoles:

$$F = \frac{\mu_0 m_1 m_2}{4\pi\mu_R r^2} \quad (1)$$

Where μ_0 and μ_R are constants corresponding to the magnetic permeability of vacuum and the relative magnetic permeability of the medium separating the poles while *r* is the distance between them. The magnetic field *B* due to a pole of strength *m* at a distance *r* from the pole is defined as the force exerted on a unit positive pole at that point [14]:

$$B = \frac{\mu_0 m}{4\pi\mu_R r^2} \quad (2)$$

Magnetic susceptibility k is a dimensionless proportionality constant that indicates the degree of magnetization of a material in response to an applied magnetic field. Magnetic susceptibility k relates the intensity of magnetization *M* to the strength of induced magnetic field *H* through the expression in equation 3.

$$k = \frac{M}{H} \tag{3}$$

It is as well possible to express the relationship between *B* and *H* in terms of magnetic susceptibility k [15].

$$B = \mu_0 H(1 + k) \tag{4}$$

On the other hand, the radiometric approach is a geophysical technique that measures the gamma rays released by the radioactive isotopes of uranium, thorium, and potassium during radioactive decay in order to estimate the amounts of these elements. The process by which an unstable atom becomes stable by nucleus decay is known as radioactivity [4]. One of the electromagnetic spectra with energy (E), frequency (f), and wavelength (λ) that moves at the speed of light (c) is gamma radiation. These are connected by:

$$E = hf \tag{5}$$

Therefore,

$$E = \frac{hc}{\lambda} \tag{6}$$

The law of radioactivity states that the reduction in the quantity of atoms of unstable nuclei with time is expressed as [2]:

$$N_t = N_0 e^{-\lambda t} \tag{7}$$

where N_t is the quantity of atoms after decay with time t(s), N_0 is the initial quantity of atoms and λ is the decay constant of the unstable nuclei (S^{-1}).

2.1.2 Methods of Data Analysis

(a) First Vertical Derivative (FVD)

This technique is usually adopted to quantify the spatial rate of change of the magnetic field in vertical direction. The first vertical derivative filter forms part of vertical filters often applied to enhance high frequency component of a magnetic data associated with shallow bodies at the expense of low frequency component associated with deep-seated bodies. It is usually estimated in the frequency domain, by multiplying the Fourier transformed data with the filter. The FVD filter as expressed as [16]:

$$FVD = \frac{\partial B}{\partial Z} \tag{8}$$

where ∂B is the derivative of the magnetic field in Z direction.

(b) Horizontal Gradient Magnitude (HGM)

The HGM is frequently used to delineate the boundaries and horizontal extent of anomalous source bodies. [17] characterizes the method as the most straightforward method of determining linear and continuous contact locations of magnetic sources, and because the mathematical expression is a square of first-order derivatives, it has a very low sensitivity to noise in magnetic data [18]:

$$HGM = \sqrt{\left[\frac{\partial B}{\partial x}\right]^2 + \left[\frac{\partial B}{\partial y}\right]^2} \tag{9}$$

Where ∂B is the derivative of the magnetic field in the directions of x and y.

(c) Tilt Derivative (TDR)

The tilt derivative is a filter employed in the frequency domain to enhance anomalies associated with shallow structures for mineral mapping. The filter is defined as the arctangent of the fraction of FVD to HGM of the magnetic field data. Mathematically, the expression can be written as [19]:

$$TDR = tan^{-1}\left[\frac{FVD}{HGM}\right] \quad (10)$$

In addition to revealing regions with anomalous features that are least impacted by noise, tilt derivative has reportedly helped estimate fault zones, dykes, and contact locations that are linear and highly continuous at depth [20]. [21] said that the inverse function of the trigonometric tangent causes the tilt angle derivative's amplitudes to vary from -π/2 to π/2 radians.

(d) Analytic Signal

The analytic signal technique is based on the use of the first derivative of magnetic anomalies to estimate source characteristics and to locate positions of near surface geologic features. The AS method is unlike the RTE, that does not require the direction of magnetization source prior to the application of the filter. Analytic Signal peaks above narrow bodies and along the edges of larger geologic features that are in magnetic contrast to their surroundings. The AS is a very useful interpretation product in areas where magnetic remanence is suspected and in areas of low latitude since it is not affected by magnetization direction. The AS filter is defined as the square root of the sum of the vertical and horizontal derivatives of magnetic field given as thus [22]:

$$A(x,y) = \sqrt{\left(\frac{\partial B}{\partial x}\right)^2 + \left(\frac{\partial B}{\partial y}\right)^2 + \left(\frac{\partial B}{\partial z}\right)^2} \quad (11)$$

where $\frac{\partial B}{\partial x}$, $\frac{\partial B}{\partial y}$ and $\frac{\partial B}{\partial z}$ are the vertical and horizontal first derivatives of the total magnetic field and $A(x,y)$ is the amplitude of the analytic signal at (x,y). B is the observed magnetic field at (x,y).

(e) Euler Deconvolution

Euler deconvolution provides depth estimation and locations of various sources in a given area based on the Euler's homogeneity equation. [23] showed that the equation could be written in the form;

$$(x-x_0)\frac{\partial B}{\partial x} + (y-y_0)\frac{\partial B}{\partial y} + (z-z_0)\frac{\partial B}{\partial z} = N(Z-B) \quad (12)$$

where $(\mathrm{x}_0, \mathrm{y}_0, \mathrm{z}_0)$ is the location of a magnetic source whose total field B is observed at $(\mathrm{x}, \mathrm{y}, \mathrm{z})$. ($\frac{\partial \mathrm{B}}{\partial \mathrm{x}}, \frac{\partial \mathrm{B}}{\partial \mathrm{y}}$ and $\frac{\partial \mathrm{B}}{\partial \mathrm{z}}$) are derivatives of the magnetic field in x, y and z directions, while Z is the regional value of the total field and N is the structural index.

(f) Potassium (K), Equivalent Thorium (eTh) and Equivalent Uranium (eU)

For the analysis, three datasets of gamma decay were utilized: Potassium, Thorium, and Uranium. The aerial radiometric data collected encompassed maps for Potassium (K), equivalent Thorium (eTh), and equivalent Uranium (eU), each illustrating the apparent surface distribution of these radioelements.

(g) Potassium-Thorium Map (K/eTh)
Hydrothermal alteration zones are identified by analyzing the Potassium-Thorium (K/eTh) ratio maps. Potassium, being relatively more mobile than thorium, tends to accumulate in altered areas while thorium remains less mobile. Regions exhibiting a K/eTh ratio greater than 0.2 %/ppm are typically indicative of hydrothermal alteration [24]. This elevated ratio reflects the preferential enrichment of potassium during the alteration process, making it a key indicator of such zones.

(h) Ternary Map
Ternary map of radioelements is crucial in mineral exploration for several reasons. It combines data from uranium (U), thorium (Th), and potassium (K), which have distinct geochemical behaviors tied to specific rock types and mineral deposits. By plotting their concentrations on a ternary diagram, different geological units can be distinguished and anomalous concentrations identified which may indicate potential mineralization zones. Ternary maps help in mapping geological structures, such as faults and alteration zones, associated with mineral deposits [25].

3.1 Materials and Methods
The materials used in this research include half degree sheets of high resolution aeromagnetic and aero-radiometric data of Ganjuwa (sheet 129), Oasis Montaj version 8.4, ArcMap version 10.8, Surfer 16 and Microsoft excel.

3.2 Data Sources and Specifications
The airborne magnetic and radiometric data of the study area were obtained from the Nigeria Geological Survey Agency (NGSA). Fugro airborne services acquired this set of data on behalf of the Nigerian Government between 2004 and 2009. The datasets were obtained with flight line intervals of 500m and flight height of 80m. Data corrections which include elimination of temporal variations, height corrections, and removal of the International Geomagnetic Reference Field (IGRF) were carried out by Fugro airborne services on the magnetic data on behalf of the agency as part of preprocessing [26].

3.3 Methods and Procedures of Data Processing
The following procedures were followed for the processing of the magnetic and radiometric data of Ganjuwa:

The acquired magnetic grid of the study area was imported into Oasis Montaj software, where the database was extracted as a Comma Separated Values (CSV) file. The CSV file underwent thorough inspection to ensure that all rows and columns were correctly positioned and there were no missing or erratic entries of x, y, or z values. Subsequently, the CSV file was re-imported into Oasis Montaj for gridding. The minimum curvature gridding technique was employed to generate the magnetic data grids. This process was carried out using the ‘Grid and Image’ dropdown in Oasis Montaj, with a grid cell size of 125 selected to avoid over or under-sampling. This resulted in the creation of the Total Magnetic Intensity (TMI) grid. The regional magnetic intensity grid was then extracted using the Polynomial filter found in the 'Database Tools' section of Oasis Montaj. Following this, the residual magnetic intensity grid was obtained through simple grid math within the program by subtracting the regional grid from the TMI grid, resulting in a grid that specifically represented residual magnetic intensity. Given the geographical location of the study area, the Reduction to the Magnetic Equator (RTE) filter was applied to the residual magnetic intensity from the MAGMAP dropdown to reposition anomaly peaks to the center of their causative bodies, resulting in the Reduction to the Equator (RTE) grid. Structural enhancement filters, including Analytic Signal (AS), First Vertical Derivative (FVD), Horizontal Gradient Magnitude (HGM), and Tilt Derivative (TDR), were applied to the RTE

grid to generate the AS, FVD, HGM, and TDR grids. This was accomplished using the MAGMAP dropdown in Oasis Montaj. The HGM grid was then superimposed on the 0-contour of the TDR grid in Oasis Montaj and exported to QGIS software, where structural lineaments were extracted based on the alignment of the 0-contour of TDR and peaks of HGM. The Euler deconvolution technique was applied to the RTE grid to estimate the depth and locations of magnetic sources, using a structural index of 1. This was performed using the Euler3D menu in Oasis Montaj. Linear structures of interest were further delineated and digitized in QGIS, then superimposed on the Euler deconvolution grid.

Radiometric data grids for potassium (K), thorium (Th), and uranium (U) concentrations were processed using Oasis Montaj software. The data was initially extracted as Comma Separated Values (CSV) files, which were then thoroughly inspected to verify that all entries were accurate and correctly positioned. Following this, the CSV files were imported back into Oasis Montaj for gridding. The minimum curvature gridding technique was utilized to create the radiometric data grids. This was executed via the 'Grid and Image' menu, with a grid cell size of 125 selected to avoid over- or under-sampling. This process resulted in the generation of separate concentration grids for K, Th, and U concentrations. To analyze the data further, a potassium/thorium ratio grid was created using the grid math tool under the 'Grid and Image' menu, by dividing the potassium concentration grid by the thorium concentration grid. Additionally, a ternary grid was produced to visually represent the concentrations of K, U, and Th, with each element color-coded in red, green, and blue, respectively and to correlate these concentrations with rock units on the geological map. This ternary grid was extracted using the ternary image tool under the 'Grid and Image' menu.

4.1 RESULTS AND DISCUSSION

The analysis of the aeromagnetic and aero-radiometric data reveals the following results

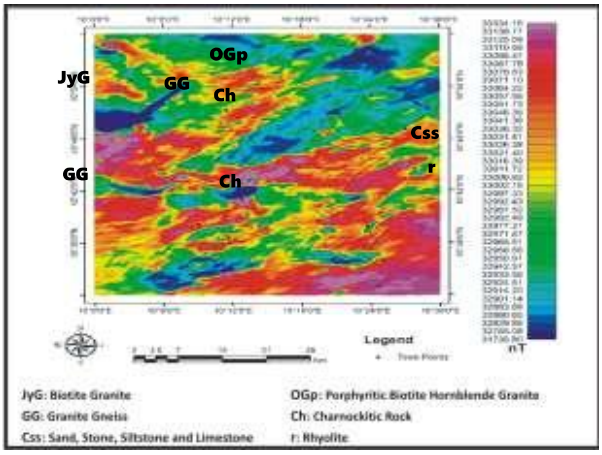

Figure 3: Total Magnetic Intensity (TMI) Map of the Study Area

The Total Magnetic Intensity (TMI) map (Figure 3) visually displays magnetic anomalies in the study area, highlighting variations in magnetic susceptibility. It shows a spectrum from strong anomalies (indicating higher concentrations of ferromagnetic minerals like iron ore) to weak anomalies (suggesting lower concentrations of diamagnetic minerals like quartz). TMI values range from 32,785.08nT (blue) to 33,334.15nT (pink).

The residual magnetic intensity map in Figure 4, displays intensity values ranging from -201.97nT (blue) to 360.07nT (pink), indicating both positive and negative magnetic

anomalies. High magnetic intensities are found in the western, eastern, southeastern, and central regions, aligning with various rock types: Porphyritic Biotite Hornblende Granite and Granite Gneiss in the east, Charnockite in the center, and Rhyolite in the southeast. Lower intensities are present in the northeastern, southwestern, central, and northwestern areas, corresponding to sandstone, siltstone, limestone, and specific granite types.

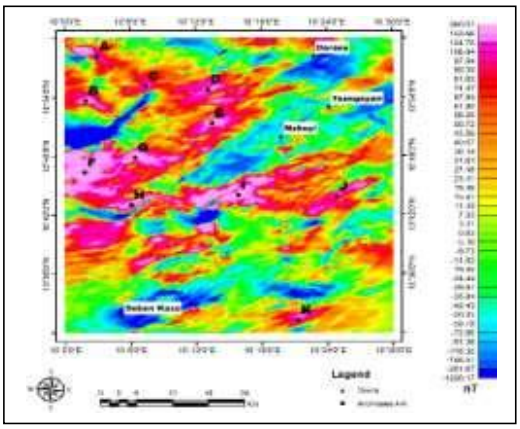

Figure 4: Residual Map

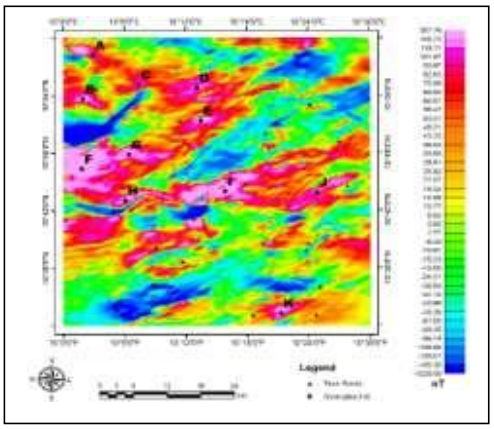

Figure 5: Reduction to the Equator Map

The residual magnetic intensity was adjusted to the equator using Oasis Montaj to better align anomalies with their sources. The reduced map (Figure 5) shows values ranging from -195.30nT (blue) to 362.26nT (pink), which are only slightly higher than those in the residual map. The adjustment did not significantly change the anomaly patterns.

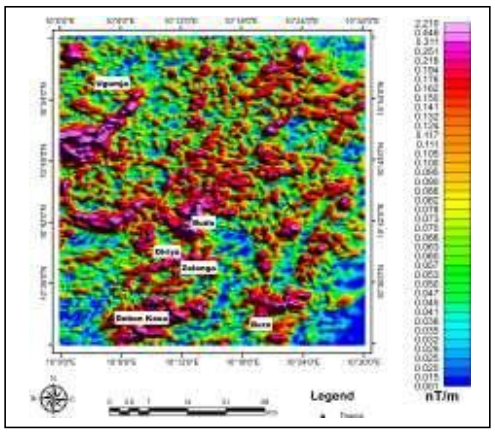

Figure 6: Analytic Signal Map

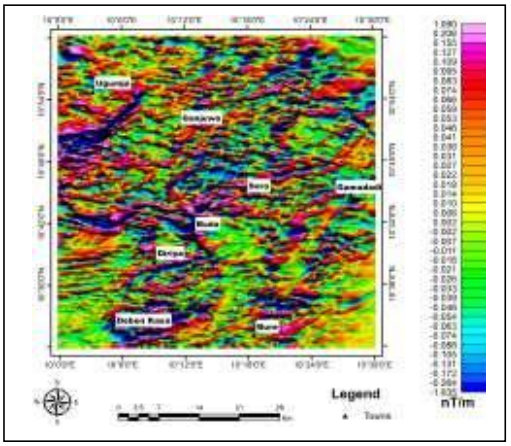

Figure 7: First Vertical Derivative Map

The analytic signal map (Figure 6) highlights magnetic source edges, with amplitudes ranging from 0.015nT/m to 2.210nT/m. High amplitude zones, indicating potential iron ore or metallic mineralization, are notably around Buda, Deben Kasa, south of Ugumja, northeast of Bure, north of Zalanga, and northwest of Diriya.

First Vertical Derivative (FVD) map in Figure 7 reveals near-surface lineaments trending SW-NE, with values ranging from -0.264nT/m (blue) to 1.09nT/m (pink). Major lineaments were identified south of Ugumja town, south of Ganjuwa town, and along Diriya, Buda, Soro,

Bure, Deben Kasa, and Gamadadi towns. These features indicate the presence of subtle magnetic structures like fractures and faults that could host magnetic minerals.

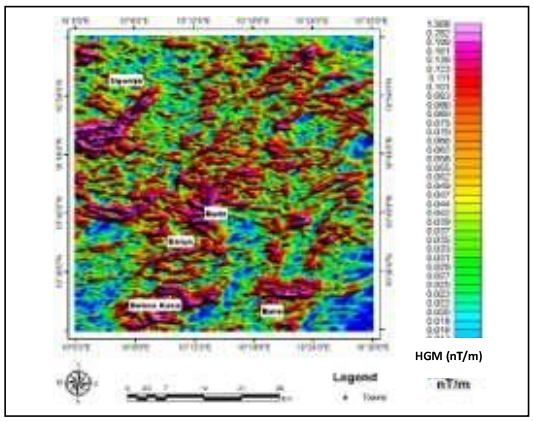

Figure 8: HGM Map

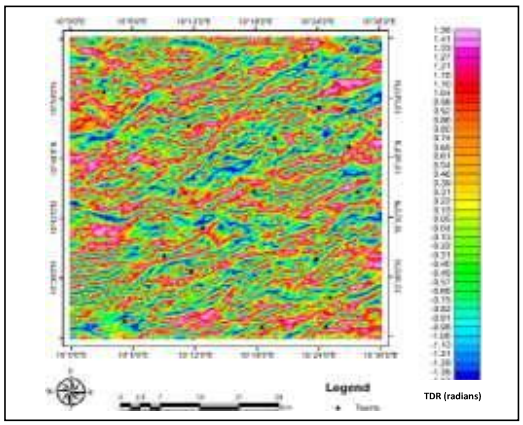

Figure 9: TDR Map

The Horizontal Gradient Magnitude (HGM) map, shown in Figure 8, exhibits patterns similar to those in the analytic signal map. It ranges from 0.006nT/m (blue) to 1.568nT/m (pink) and highlights lineaments trending SW-NE. Key features are found south of Ugumja town, north of Bure town, and around Buda, Diriya, and Deben Kasa towns.

The Tilt Derivative (TDR) map shown in Figure 9 reveals values, ranging from -1.38rad (blue) to 1.56rad (pink) and highlights NE-SW trending linear features as seen in analytic signal and FVD maps in Figure 6 and Figure 7.

The Horizontal Gradient Magnitude (HGM) map in Figure 8 was overlaid on the Tilt Derivative (TDR) 0-contours to assess the correlation between linear features on the maps. The resultant lineaments map in Figure 10 reveals lineaments that are generally distributed across the study area, with major trends in the northwestern, central, and southern regions, predominantly in the NE-SW direction.

The Euler deconvolution map, shown in Figure 11, highlights trends and edges of dykes and sills, predominantly in the NE-SW direction. Depths ranges from 122.47m to 1102.75m, with most of the delineated structures between 500m and 750m in red and 250m to 500m in green. These results align well with the delineated lineaments in Figure 6 and Figure 7.

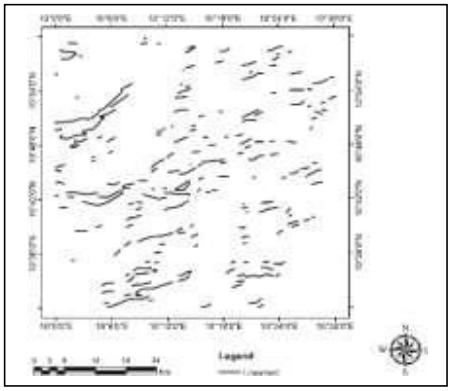

Figure 10: Lineaments Map

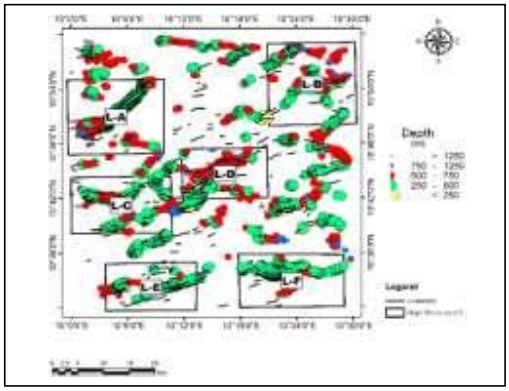

Figure 11: Euler Deconvolution Map

Table 1: Correlation of Some Linear Structures to their Respective Depth Ranges, Location and Geology of the Study Area

Rock type	Linear structure	Depth range (m)	Direction
JyG, OGP, GG	L-A	130-750	NW
OGp, Css	L-B	250-1100	NE
OGp, GG	L-C	130-750	SW
OGp, Ch	L-D	250-1100	C
OGp, Ch	L-E	250-750	SW
OGp, Css, r	L-F	250-750	SE

Key: Biotite granite (JyG), Porphyritic biotite hornblende granite (OGp), Granite gneiss (GG), Charnockitic rock (Ch), Sand, stone siltstone and limestone (Css), Northwest (NW), Southwest (SW), Central (C), East (E), Southeast (SE).

Table 1 gives the location of some lineaments of interest, L-A to L-F, together with their corresponding depths. L-A and L-C are observed in the northwestern and southwestern regions of the study area and have depths ranging from 130m-750m. L-E and L-F have depths ranging from 250m to 750m and are located in the southwestern and southeastern regions of the study area. L-B and L-D have the deepest depths ranging from 250m to 1100m and are located in the northeastern and central regions of the study area.

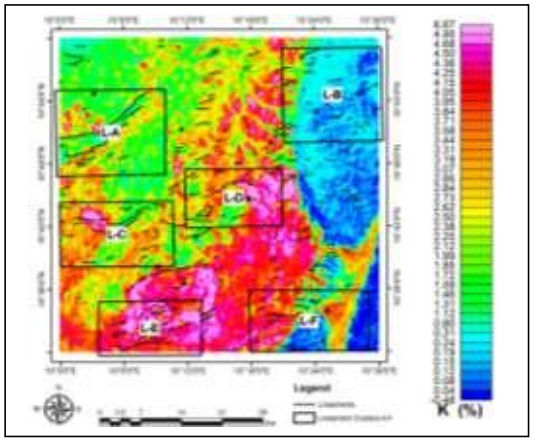

Figure 12: Potassium (K) Concentration Map

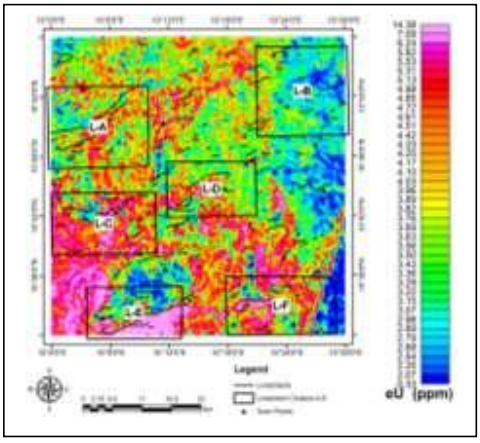

Figure 13: Uranium (eU) Concentration Map

Figure 12 shows potassium distribution in the study area. Low concentrations (0.04 to 1.12%) are primarily seen in the eastern region (blue). Medium concentrations (1.31 to 3.71%) are concentrated in the western and northwestern areas (green, yellow, orange). High concentrations (3.84 to 6.67%) are mainly in the southern region (deep red, pink).

Figure 13 illustrates uranium concentrations ranging from 2.07 ppm (blue) to 14.38 ppm (pink). The highest concentrations are found in the southern and northwestern regions, while the lowest concentrations are primarily in the eastern region and northeast of Deben Kasa town.

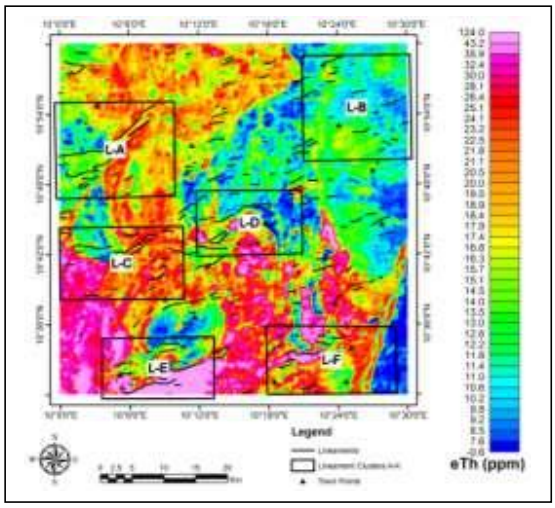

Figure 14: Thorium (eTh) Concentration Map

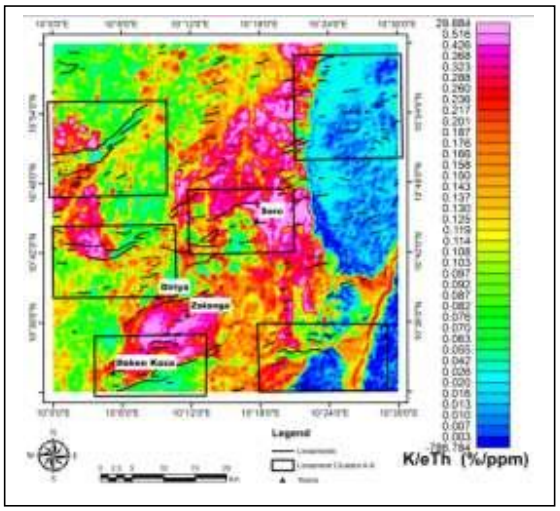

Figure 15: K/eTh Ratio Map

Figure 14 shows thorium concentration in the study area, ranging from 7.6 ppm to 124 ppm. The highest concentrations (pink) are in the southern and southwestern regions, while the lowest concentrations (blue) are mainly in the eastern region.

Figure 15 shows the potassium-thorium (K/eTh) ratio, with values ranging from 0.003 (blue) to 29.884 (pink). Higher ratios, indicating K enrichment, are predominantly found in the northeastern and central regions, extending to Soro town. Additional K-enriched areas are located in the southern region around Zalanga, Diriya, and Deben Kasa, and in patches in the western region between latitudes 10°40'N to 10°54'N and longitudes 10°00'E to 10°06'E.

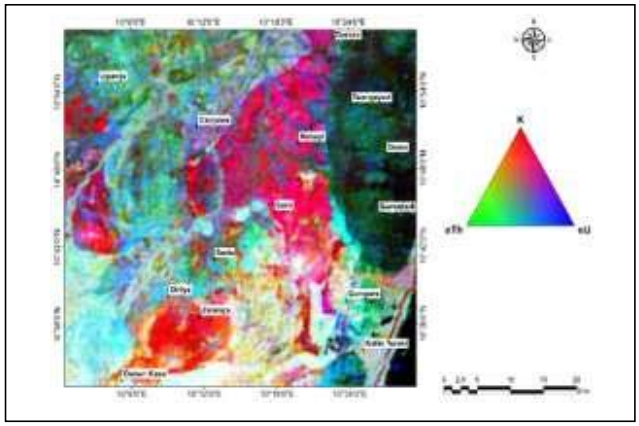

Figure 16: Ternary Map of the Study Area

Figure 16 presents a ternary map showing the relative abundances of potassium (K), uranium (U), and thorium (Th). White areas indicate high concentrations of all three elements, while dark colors represent low concentrations. Red signifies K dominance, green indicates high Th, and blue highlights high U. The map shows high U and Th in the western and southeastern regions, high K with low Th and U in the central and southern regions, and low concentrations of all three elements in the eastern region. The southern and southwestern areas feature high concentrations of K, Th, and U.

Table 2: Quantitative Description of Concentration Levels of the Three Radioelements (K, Th and U) and their Ratios (K/eTh)

K (%)	eTh (ppm)	eU (ppm)	K/eTh (%/ppm)
L (0.04-1.12)	L (7.6-11.8)	L (2.07-3.15)	L (≤ 0.05)
M (1.31-3.71)	M (12.2-22.5)	M (3.22-4.72)	M (0.06-0.20)
H (3.84-6.67)	H (23.2-124)	H (4.85-14.38)	H (0.217-29.88)

Key: High (H), Medium (M), Low (L)

Table 2 gives the quantitative description of the concentration levels of the three radionuclides (K, eTh and eU) and the ratio (K/eTh) as obtained from their concentration maps in Figures 12-14 and the ratio map in Figure 15.

Table 3: Comparison of Radionuclide Concentrations: Study Area Versus Global Averages and Safety Limits [27]

Radionuclide	Average Abundance in the study area	Average global Abundance	Deviation	Average safe value
K (%)	3.6	2.5	1.1	2
eTh (ppm)	15.4	10	5.4	< 20
eU (ppm)	8.2	2.8	5.4	< 30

Table 3 compares the average radionuclide concentrations in the study area with global averages and safety limits. Potassium averages 3.6% in the study area, higher than the global average of 2.5%, but this increase is not considered hazardous. Thorium averages 15.4 ppm, exceeding the global average of 10 ppm but remaining below the safe limit of 20 ppm, indicating possible localized mineralization. Uranium averages 8.2 ppm, significantly above the global average of 2.8 ppm but below the safe limit of 30 ppm, suggesting potential radioactive mineralization in the region.

Table 4 analyzes the spatial relationship between high concentrations of radionuclides, their ratios, and corresponding linear structures from aeromagnetic data. It identifies potential zones of radioactive mineralization by correlating these features. High potassium (3.84% to 6.67%) is found primarily in the southern region, aligning with linear structures L-E and L-D, which have depths of 250m to 1100m. Elevated uranium (4.85ppm to 14.38ppm) and thorium (23.2ppm to 124ppm) concentrations are in the southwestern region, correlating with linear structures L-C and L-E, with depths of 130m to 750m.

Table 4: Integration of Delineated Linear Features (L-A to L-F) with Highest Concentrations of Radionuclides Together with their Respective Locations and Depths

Radionuclides and their ratios	Highest Concentration	Linear structure	Depth (m)	Location
K (%)	3.84-6.67	L-E and L-D	250-1100	S
eU (ppm)	4.85-14.38	L-C and L-E	130-750	SW
eTh (ppm)	23.2-124	L-C and L-E	130-750	SW
K/eTh (%/ppm)	0.217-29.88	L-D and L-E	250-1100	C and SW

Key: Central (C), South (S), Southwest (SW)

A highly concentrated region for possible thorium (Th) and uranium (U) exploitation is identified in the southern region of the study area, between latitudes 10°30'N to 10°33'N and longitudes 10°03'E to 10°15'E, with depths ranging from 130m to 750m as seen in Table 4, Figure 13, Figure 14 and Figure 11. Ratio map for potassium/thorium (K/eTh) highlights hydrothermal alteration zones indicated by potassium enrichment and thorium depletion. These alteration zones, mostly in the western, southwestern, and central regions, correspond to lineaments L-E and L-D, and are potential targets for further exploration as observed in the same table.

5 Conclusions

The geophysical delineation of radioactive mineralization in Ganjuwa area of Bauchi state, northeastern Nigeria, was conducted using aeromagnetic and aero-radiometric data. The analysis revealed a broad spectrum of magnetic intensities, ranging from -201.97nT to 360.07nT, with moderate to high values predominantly in the central and eastern regions, indicating a complex magnetic environment. Structural enhancement methods identified NE-SW trending linear features, correlating with significant geological structures, while Euler deconvolution depth estimates ranged from 122.47m to 1102.75m. Radiometric data indicated varied concentrations of radionuclides corresponding to Porphyritic Biotite Hornblende Granite and Granite Gneiss rock units. Potassium levels ranged from 0.04% to 6.67%, thorium from 7.6 ppm to 124 ppm, and uranium from 2.07 ppm to 14.38 ppm. These concentrations, although elevated relative to global averages, remain within safe limits and do not pose significant health risks. Prominent areas of potential mineralization are generally identified in the southern region of the study area. These radioactive mineralization zones correspond with lineament clusters L-C, L-D, and L-E, which indicate that they are structurally controlled. Notable areas of potassium (K) mineralization are located between latitudes 10°30'N to 10°47'N and longitudes 10°03'E to 10°22'E, with depths from 250m to 800m. Thorium (Th) and uranium (U) mineralization zones were observed between latitudes 10°30'N to 10°43'N and longitudes 10°00'E to 10°18'E, with depths ranging from 130 m to 750 m. Hydrothermal alteration zones are identified between latitudes 10°32'N to 11°00'N and longitudes 10°04'E to 10°24'E, with depths from 250m to 800m. This comprehensive assessment underscores significant geological features and potential radioactive mineralization zones in Ganjuwa for exploitation and further exploration. The findings provide a robust foundation for targeted exploration and development strategies.

Acknowledgments

The author would like to thank NGSA for the availability of data.

Conflict of Interest

The research team declares that they have no conflict of interest.

References

[1] A. Arogundade *et al.*, “Integrated Aeromagnetic and Airborne Radiometric Data for Mappin g Potential Areas of Mineralisation Deposits in Parts of Zamfara , North West Nigeria,” *Pure Appl. Geophys.*, vol. 7, no. 3, pp. 021–039, 2022, doi: 10.1007/s00024-021-02913-w.

[2] L. William, *Fundamentals of Geophysics*, Second Edi. Zurich, Switzerland: Cambridge University Press, 2007.

[3] P. Kearey, M. Brooks, and I. Hill, *An Introduction to Geophysical Exploration*, Third. Great Britain: Blackwell Publishing, 2002.

[4] W. Telford, L. Geldart, and R. Sheriff, *Applied Geophysics*, Second Edi. United Kingdom, Cambridge: Cambridge University Press, 1990.

[5] A. Usman, A. Lawan, M. Lawal, L. Jonathan, and S. Sununu, "Structural Analysis of Selected Ring Complexes in Some Parts of the Nigerian Younger Granite Provinces," *Saudi J. Eng. Technol.*, vol. 6272, no. 7, pp. 467–475, 2021, doi: 10.36348/sjet.2021.v06i12.004.

[6] J. Milsom and A. Eriksen, *Field Geophysics*, Fourth. Oxford, United Kingdom: John Willey & Sons, Ltd, 2011.

[7] A. Richard *et al.*, "Airborne magnetic and radiometric mapping for litho-structural settings and its significance for bitumen mineralization over Agbabu bitumen-belt southwestern Nigeria," *J. African Earth Sci.*, vol. 180, no. August 2020, p. 104222, 2021, doi: 10.1016/j.jafrearsci.2021.104222.

[8] I. Abubakar, N. Kure, H. Daniel, C. Afuwai, and N. Auwal, "Determination of Geothermal Potential in Yankari Game Researve, Bauchi State, Nigeria," *FUDMA J. Sci.*, vol. 7, no. 1, pp. 103–109, 2023, doi: doi.org/10.33003/fjs-2023-0701-1254.

[9] A. . Chinwuko, A. . Onwuemesi, E. . Anakwuba, L. . Onuba, and N. . Nwokeabia, "Interpretation of Aeromagnetic Anomalies over parts of Upper Benue Trough Interpretation of Aeromagnetic Anomalies over parts of Upper Benue Trough and Southern Chad Basin , Nigeria," *Adv. Appl. Sci. Res.*, vol. 3, no. 3, pp. 1757–1766, 2012, doi: 346.8574.23445.

[10] A. Yusuf, L. H. San, and I. A. Abir, "A Preliminary Geothermal Prospectivity Mapping Based on Integrated GIS , Remote-Sensing , and Geophysical Techniques around Northeastern Nigeria," *MPDI J. Environ. Sustain.*, vol. 13, no. 8, pp. 726–734, 2021, doi: 10.3390/su13158525.

[11] S. E. Ekwok, A. E. Akpan, E. D. Ebong, and O. E. Eze, "Assessment of depth to magnetic sources using high resolution aeromagnetic data of some parts of the Lower Benue Trough and adjoining areas , Southeast Nigeria," *Adv. Sp. Res.*, vol. 67, p. 2119, 2021.

[12] N. N. Eluwa, A. I. Opara, C. N. Okereke, C. Eluwa, and R. M. Onwe, "Estimation of radioelements concentration in Sokoto Basin for geothermal energy studies using airborne radiometric data," *World J. Adv. Res. Rev.*, vol. 12, no. 1, pp. 315–325, 2021, doi: 10.30574/wjarr.2021.12.1.0514.

[13] A. A. Adepelumi and A. H. Falade, "Combined high-resolution aeromagnetic and radiometric mapping of uranium mineralization and tectonic settings in Northeastern Nigeria," *Acta Geophys.*, vol. 65, no. 5, pp. 1043–1068, 2017, doi: 10.1007/s11600-017-0080-3.

[14] J. (Reynolds I. L. Reynolds, *An Introduction to Applied and Environmental Geophysics*, Second. West Sussex, United Kingdom: John Wiley & Sons Ltd, 2011. [Online]. Available: www.wiley.com/wiley-blackwell

[15] F. Stacey and P. Davis, *Physics of the Earth*, Fourth. Cambridge, United Kingdom: Cambridge University Press, 2008. [Online]. Available: www.cambridge.org/9780521873628

[16] F. N. Okeke, D. Obiora, and S. Taufiq, "Interpretation of aeromagnetic data over some parts of Sokoto Basin , Nigeria , using source parameter imaging and 3D Euler deconvolution methods," *Int. J. Phys. Sci.*, vol. 15, no. July, pp. 90–98, 2020, doi: 10.5897/IJPS2020.4864.

[17] T. O. Lawal, J. Sunday, M. Salami, J. Sunday, K. Fawale, and T. Adewumi, "Use of Magnetic anomaly data to delineate subsurface structures and depth characterization of Lafiagi and its environs , Northcentral Nigeria," *NRIAG J. Astron. Geophys.*, vol. 10, no. 1, pp. 157–169, 2021, doi: 10.1080/20909977.2021.1900526.

[18] D. Dahuwa, W. Umar, M. Sani, and L. Abba, "Aeromagnetic data analysis of tafawa balewa area using second vertical derivative and analytic signal techniques," *IOSR J. Appl. Geol. Geophys.*, vol. 6, no. 1, pp. 25–32, 2018, doi: 10.9790/0990-

0601012532.
[19] A. Nda, Y. A. Sanusi, S. B. Mohammad, and A. Roko, “Application of Aeromagnetic Data Analysis and Interpretations to Investigate Solid Mineral Potential in Part of Northwest Nigeria,” *Int. J. Earth Sci. Geophys.*, vol. 10, no. 7, pp. 2631–5033, 2022, doi: 10.35840/2631-5033/1857.
[20] M. Bersi and H. Saibi, “Aerogravity and remote sensing observations of an iron deposit in Gara Djebilet , southwestern Algeria,” vol. 116, no. April, 2016, doi: https://doi.org/10.1016/j.jafrearsci.2016.01.004.
[21] C. Ozebo, O. Ogunkoya, O. Layade, and L. Bisilimi, “Evaluation of Aeromagnetic Data of Ilesha Area of Oyo State Nigeria using Analytical Signal (ASM) and Local wavenumber (LWN),” *J. Aplplied Sci. Environ. Manag.*, vol. 21, no. 6, pp. 1157–1161, 2017, doi: 10.4314/jasem.v21i6.28.
[22] A. Augie and O. Ologe, “Analysis of Aeromagnetic Data For Coal Deposit Potential Over Birnin Kebbi and Its Environs, Northwestern Nigeria,” *Niger. J. Sci. Environ.*, vol. 18, no. 1, pp. 144–153, 2020, doi: 10.1080/20909977.2021.1900526.
[23] A. B. Mohammed and R. Jimoh, “Characterization of Gold Mineralization Zones using Aeromagnetic Data at Dutsen Dan-Baqoshi , Dushi Area of Kano State , Northwestern Nigeria,” vol. 5, no. 2, pp. 121–133, 2019.
[24] F. Abubakar, S. Ibrahim, and C. Egemba, “Investigation of iron ore potential in north-central Nigeria , using high-resolution aeromagnetic dataset and remote sensing approach,” *Heliyon J. Geosci.*, vol. 10, no. 1, p. 32, 2024, doi: doi.org/10.1016/j.heliyon.2023.e23618.
[25] C. Nwokeabia, A. Opara, O. Ibe, and B. Odoh, “Correlation of Radiation Doses from Radiometric data and Aero- magnetic Signatures over Parts of Southeastern Nigeria,” *J. Mater. Environ. Sci.*, vol. 14, no. January, pp. 475–490, 2023, [Online]. Available: https://www.researchgate.net/publication/370403938%0ACorrelation
[26] (NGSA) Nigeria Geological Survey Agency, “Aeromagnetic Survey Specifications,” 2005.
[27] K. Chandrashekara and H. M. Somashekarappa, “Estimation of radionuclides concentration and average annual committed effective dose due to ingestion for some selected medicinal plants of South India,” *J. Radiat. Res. Appl. Sci.*, vol. 9, no. 1, pp. 68–77, 2016, doi: 10.1016/j.jrras.2015.09.005.